PROCEEDINGS A

royalsocietypublishing.org/journal/rspa

Research



Cite this article: Shuang F, Xiao P, Xiong L, Gao W. 2022 Atomistic mechanisms of phase nucleation and propagation in a model two-dimensional system. *Proc. R. Soc. A* **478**: 20220388.

https://doi.org/10.1098/rspa.2022.0388

Received: 9 June 2022

Accepted: 10 November 2022

Subject Areas:

computational chemistry, computational mechanics, materials science

Keywords:

phase transition, nucleation, defects, nudged elastic band, dimer

Author for correspondence:

Wei Gao

e-mail: wei.gao@tamu.edu

Electronic supplementary material is available online at https://doi.org/10.6084/m9.figshare. c.6316500.

Atomistic mechanisms of phase nucleation and propagation in a model two-dimensional system

Fei Shuang¹, Penghao Xiao³, Liming Xiong⁴ and Wei Gao^{1,2}

¹Department of Mechanical Engineering, The University of Texas at San Antonio, San Antonio, TX 78249, USA

²J. Mike Walker '66 Department of Mechanical Engineering, Texas A&M University, College Station, TX 77843, USA

³Department of Physics and Atmospheric Science, Dalhousie University, Halifax, Nova Scotia, Canada B3H 4R2

⁴Department of Aerospace Engineering, Iowa State University, Ames, IA 50011, USA

We present a computational study on the solid-solid phase transition of a model two-dimensional system between hexagonal and square phases under pressure. The atomistic mechanism of phase nucleation and propagation are determined using solid-state Dimer and nudged elastic band (NEB) methods. The Dimer is applied to identify the saddle configurations and NEB is applied to generate the transition minimum energy path (MEP) using the outputs of Dimer. Both the atomic and cell degrees of freedom are used in saddle search, allowing us to capture the critical nuclei with relatively small supercells. It is found that the phase nucleation in the model material is triggered by the localized shear deformation that comes from the relative shift between two adjacent atomic layers. In addition to the conventional layerby-layer phase propagation, an interesting defectassisted low barrier propagation path is identified in the hexagonal to square phase transition. The study demonstrates the significance of using the Dimer method in exploring unknown transition paths without a priori assumption. The results of this study also shed light on phase transition mechanisms of other solid-state and colloidal systems.

royalsocietypublishing.org/journal/rspa Proc. R. Soc. A 478: 20220388

1. Introduction

Pressure-dependent structural phase transition appears in a broad range of materials. A typical example is bulk silicon which undergoes a series of sequential phase transitions under hydrostatic pressure [1]. In addition to solid-state materials, phase transition has also been demonstrated in many soft matter systems. For example, nanoparticles or colloidal particles can be self-assembled inside polymeric solvents to form a variety of interesting structural phases, many of which are exhibited in the form of two-dimensional or quasi-two-dimensional [2–4]. On the other side, many model two-dimensional systems have been utilized to study novel phase transition process, guiding the experimental discovery of new mechanisms in realistic materials [5–8]. In this article, we study the structural phase transition between square and hexagonal phases in a model two-dimensional system that is described by a modified Lennard–Jones (LJ) potential. Due to its simplicity, this model material is used to demonstrate a computational approach that combines solid-state Dimer and nudged elastic band (NEB) methods to determine the kinetics of nucleation and propagation process. Particularly, we want to demonstrate the significance of using the solid-state Dimer method to determine unexpected transition paths, when both atomic and cell degrees of freedom are used in saddle point searching.

Phase nucleation and propagation are rare events, i.e. much slower than atomic vibrations. Because of this, conventional molecular dynamics (MD) simulations were often conducted at pressures several times higher than in experiments so that a transition can be observed in the accessible simulation time scale [9]. The disadvantage of such an approach is that the mechanism may change with increasing pressure. Computation methods like parallel replica dynamics [10] and metadynamics [11] have been proposed to accelerate rare events sampling in MD. For example, NPT metadynamics simulation was applied in a recent article to study the pressureinduced structural phase transition in NaCl [12]. Instead of MD, the methods for computing saddle points and minimum energy path can be used to study the kinetics of nucleation and propagation [13]. One commonly used method is the NEB, which has been used to study solidsolid phase transitions [14-17]. The conventional NEB [18,19] only takes atomic positions as transition variables. A generalized solid-state NEB [20] was proposed to treat the atomic and lattice variables on an equal footing, so that phase transitions involving changes in all degrees of freedom are properly described. Recently, such solid-state NEB was slightly modified by adding finite deformation variables for more accurate evaluation of barriers and MEPs of solids subjected to finite deformation [21,22]. In the NEB, a set of images is placed between the given initial and final configurations, which are connected by springs to ensure even spacing. The optimization by reducing the force acting on the images brings the elastic band to the MEP. There are two major limitations in the NEB. Firstly, the NEB tends to converge into the MEP that is close to the initial guess, such that NEB results depend on the construction of initial images and the MEP with a lower barrier may be missed. Secondly, a final configuration must be provided to initiate NEB calculation. However, in some studies like phase nucleation and propagation in a large system, it is not convenient to choose a proper final state and an initial band. In some cases, like the one shown in this article, the final state and initial bands that appear to be reasonable could bias the search for a low barrier MEP, leading to an inaccurate phase transition path.

The Dimer method is a single-ended type of approach for finding saddle points of transition events [23]. Unlike the NEB, the Dimer starts from a given initial configuration and searches for the nearby saddle points without knowing a final configuration. In the Dimer method, two replicas of the system called a 'dimer' are rotated around its centre to find the lowest curvature mode without calculating the Hessian matrix. Then the dimer climbs up the potential energy surface along the lowest curvature mode direction while descending along all the other directions, and converges to a first-order saddle point. The corresponding final configuration can be easily obtained by relaxing the saddle configuration along the dimer direction. Like the solid-state NEB, a solid-state Dimer was developed to account for both atomic and cell degrees of freedom [24], which has shown many successful applications, such as the concerted phase transition mechanisms [24], surface processes [25,26], the migration mechanisms of dislocation

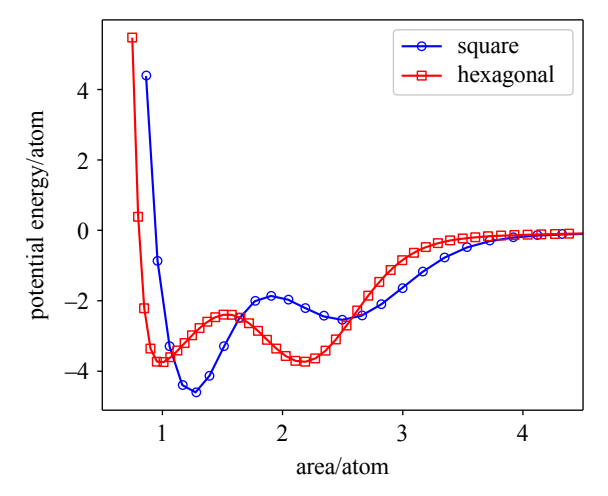


Figure 1. Empirical potential used to describe the atomic interactions in the model two-dimensional system. (Online version in colour.)

kinks in a silicon crystal [27] and so on. In this article, we apply the solid-state Dimer method, in combination with solid-state NEB, to probe the atomistic mechanism of phase nucleation and propagation. It is noted that, in addition to NEB and Dimer, there are many other types of saddle search methods, such as string method [28,29], saddle dynamics and solution landscape [30,31] and so on. A more extensive review on the methods can be found in references [32–34].

2. Two-dimensional model system

The two-dimensional system is described by a modified LJ potential:

$$V(r) = -4\varepsilon \left[\left(\frac{\sigma}{r} \right)^6 - \left(\frac{\sigma}{r} \right)^{12} \right] - G e^{-(r-r_0)^2/\lambda^2}, \tag{2.1}$$

where r is the distance between two atoms, ε and σ are the parameters of the traditional LJ potential, G=1, $\lambda=0.2$ and $r_0=1.6$ based on [6], all with reduced LJ units in terms of ε and σ . As such, all quantities are unitless. A cutoff 4.5 is adopted for both LJ and Gaussian terms. This potential describes two stable lattice structures: square and hexagonal phases. The variation of potential energies with respect to area per atom (i.e. the area of the computation cell divided by the number of atoms in the cell) is plotted in figure 1. It is seen that there exist two minima for each phase, corresponding to two stable structures with different equilibrium spacing. Our study only focuses on the phase transition between the first minima of square and hexagonal phases. Without pressure, the potential energy of square phase is lower than that of hexagonal phase, meaning that the square phase is more stable, so the transition from hexagonal to square phase is possible. As shown later in §3, when pressure increases beyond a critical pressure, the hexagonal phase becomes more stable, promoting the transition from square to hexagonal phase. It is worth noting that Damasceno $et\ al.$ studied the same two-dimensional system with MD simulation [6], but the phase nucleation and propagation mechanisms are missed in their study.

3. Results and discussion

In this section, we study the phase transition of the model two-dimensional system with a combined NEB and Dimer method. Firstly, the concerted phase transition is studied in small unit cells, demonstrating the contribution of both cell and atomic degrees of freedom to the concerted mechanism. Then, more interesting phase nucleation and propagation mechanisms are investigated using a super cell that contains 256 atoms. All the calculations are performed by the

royalsocietypublishing.org/journal/rspa Proc. R. Soc. A 478: 20220388

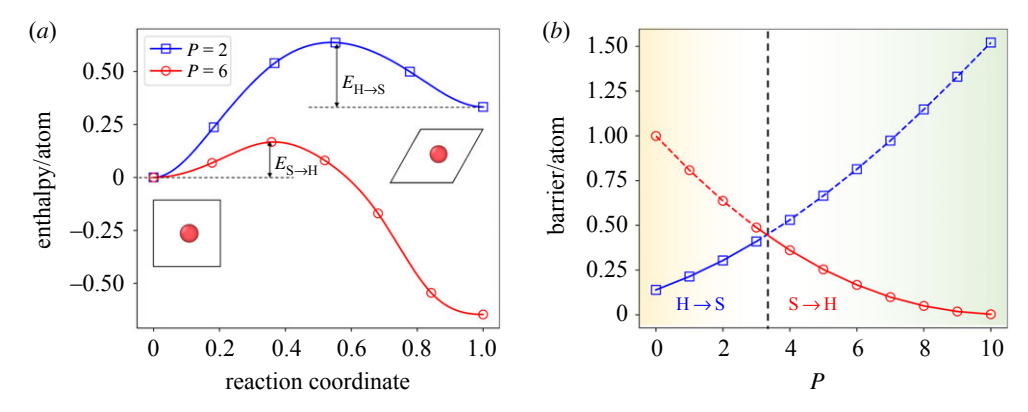


Figure 2. Phase transition in the primitive cell: (a) MEPs at P=2 and 6. Insets give the initial and final configurations. (b) Transition barriers at different pressures.

open source python packages Atomic Simulation Environment (ASE) [35] and the Transition State Library for ASE (TSASE). Potential energy, atomic force and stress are calculated by the software LAMMPS [36]. Both NEB and Dimer calculation are considered to be converged when the total force vector has a norm below 0.001. In the Dimer calculations, random perturbation that follows a normal distribution with a standard deviation of 0.005 is applied to both atoms and cell to drive the system away from the initial minima. It is noted that we run Dimer calculations hundreds of times from local minima with a variety of initial perturbations, following the procedure used in adaptive kinetic Monte Carlo method [37]. It is still not guaranteed that all the paths have been exhausted, but the important ones have been identified. The purpose of combining Dimer and NEB to find the nucleation and propagation mechanism is twofold. Firstly, NEB can be used to efficiently probe a particular transition pathway corresponding to the mechanism of interest, while Dimer is able to search many possible pathways and provide the most favourable one. Secondly, the saddle and final states identified by Dimer can be used by NEB to determine a complete MEP, where the initial guessed path used in NEB is linear interpolated from the initial state to the saddle point and from saddle point to the final state. All atomistic configurations are visualized by the software OVITO [38].

Concerted phase transition

The model two-dimensional system has a monatomic lattice, with the basis consisting of a single atom. Figure 2a shows the minimum energy path (MEP) of the phase transitions at two typical pressures, obtained from NEB calculation using a primitive cell. The square to hexagonal $(S \rightarrow H)$ transition occurs at high pressure, while the reverse transition $(H \rightarrow S)$ occurs when the pressure drops. The transition barriers calculated at different pressures are plotted in figure 2b. A critical pressure is found around P = 3.4, at which the barrier of $(S \to H)$ equals that of $(H \to S)$ and the enthalpy of the two phases is the same. Note that the primitive cell only contains a single atom, so the instability during phase transition is solely contributed by the cell degree of freedom.

Next, we use a two-atom unit cell to reveal the instability coming from the atomic degree of freedom in addition to the cell degree of freedom. The NEB results are shown in figure 3, where a representative MEP is plotted with black dashed line in figure 3a and the corresponding initial, saddle and final structures are shown in figure 3c. The reaction coordinate in MEP represents the normalized distance between the neighbouring states in terms of atom position and cell deformation. The MEP shows that the transition is mainly contributed by the relative shift between two atoms in the unit cell, accompanied by a small volumetric deformation of the cell without tilt. The barriers of this single-step transition are plotted in figure 3b, whose values are slightly lower than those for the primitive cell (plotted in figure 2b) due to different transition mechanisms. It is noted that, different from NEB results, the Dimer calculation finds another two

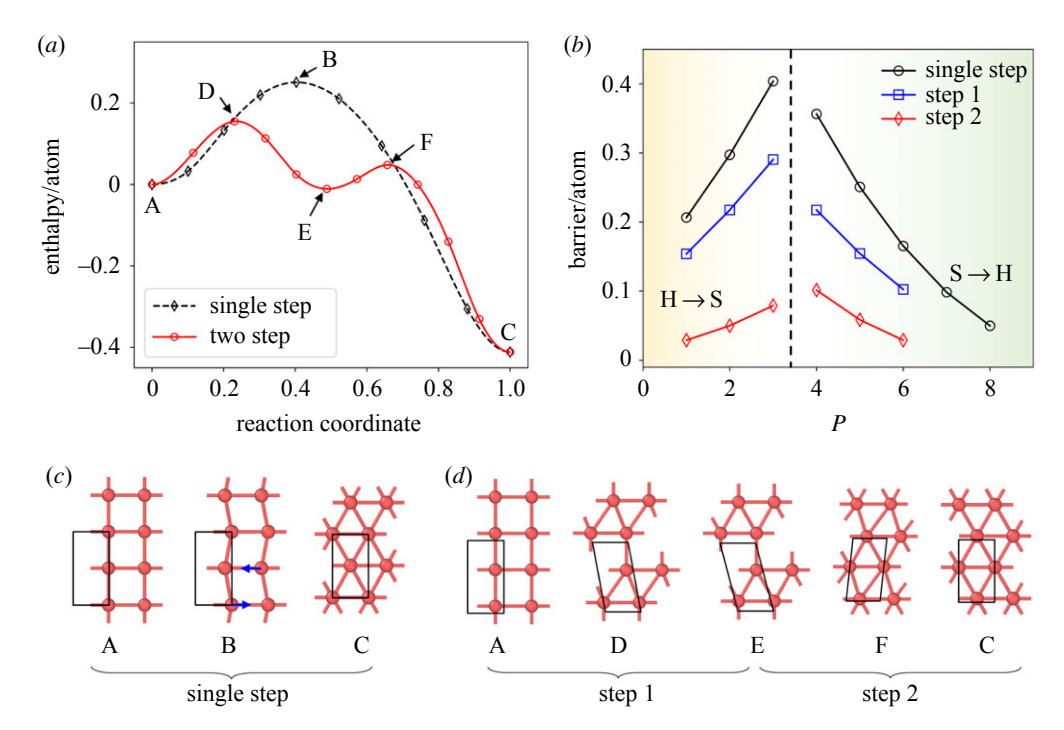


Figure 3. (a) MEPs obtained from NEB calculations at P = 5. (b) Comparison of the barriers for the single-step and two-step transitions. (c) Initial, final and saddle states in the single-step transition. (d) Initial, final, saddles and intermediate minimum in the two-step transition. (Online version in colour.)

saddle points with lower barriers: structures D and F shown in figure 3d. A relaxation of these two saddle points along the dimer direction yields the corresponding final states (structures E and C). Subsequently, a new MEP, obtained from another two NEB calculations using the Dimer results, is plotted in figure 3a with a solid red line. This new MEP shows that the phase transition of the unit cell is a two-step process: one layer of square phase first transforms into hexagonal phase, followed by the other layer. The barriers for steps 1 and 2 are plotted in figure 3b. It shows that the barriers for step 1 are much lower than that of single-step transition, meaning that the two-step transition is more kinetically favourable. However, when P > 6, the second barrier of the two-step transition approaches zero, so the concerted $S \to H$ transition can be simply finished in a single step.

Note that the two-step transition is firstly missed in the NEB calculation, so we next explain the reason for this. One worthy observation in figure 3c is that the cells of all intermediate images always retain an orthogonal shape in the NEB calculation, which indicates that a cell's angular degree of freedom is not activated in optimization when shear stress in absent. To get rid of this confinement, we can slightly disturb the cell shape of the initial images by adding 0.01 tilt degree. With this cell perturbation, the NEB is able to find the local minimum structure E in figure 3d and yield the same double-hump shaped MEP as shown in figure 3a. We tested a range of perturbations between 0.01 and 5 degrees, in which all NEB calculations could converge and lead to such a two-step transition, meaning that the NEB calculation is not sensitive to the choice of perturbation. However, when the perturbation is too large (e.g. 10°), NEB could not converge to a meaningful MEP.

The barriers calculated for the concerted phase transition increase linearly with the number of atoms in materials, thereby the concerted transition is practically possible in macroscopic materials only when the barriers are close to zero. In this kind of zero-barrier phase transition, all unit cells transform to a new phase simultaneously. By contrast, the other type of phase transition is nucleation based, in which the phase transition starts from a nucleation due to a localized

royalsocietypublishing.org/journal/rspa *Proc. R. Soc. A* **478**: 20220388

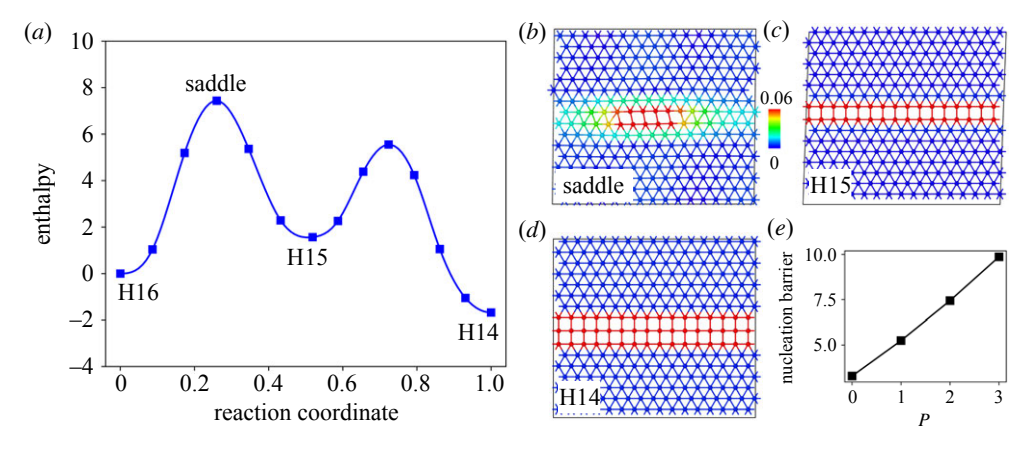


Figure 4. (a) The MEP of H oup S nucleation process at P = 2, which starts with 16 layers of hexagonal phase (H16) and bypasses an intermediate local minimum (H15) before reaching a stable nucleus (H14). (b-d) The structures of saddle, H15 and H14, where atoms are coloured by shear strain. (e) The nucleation barrier as a function of pressure. (Online version in colour.)

instability in materials, followed by a process of phase propagation. The nucleation barriers are calculated in a large super cell with many atoms, so that the calculated barriers can be used for macroscopic materials. Such nucleation-based phase transition is kinetically possible when the nucleation barrier can be overcome by external excitations such as thermal fluctuation; therefore, it is more likely to occur than the concerted phase transition. In the next two sections, we discuss the phase nucleation and propagation in the model two-dimensional system.

(b) Phase nucleation and propagation at low pressure: hexagonal to square

In this section, we focus on the $H \rightarrow S$ phase nucleation and propagation at low pressure in a periodic supercell containing 256 atoms. Note that the final configuration after nucleation is not known in advance, and we therefore need to use the Dimer method to identify the saddle and final states of the nucleation. After that, NEB is applied to generate MEP with the outputs from Dimer calculation. Figure 4a shows one representative MEP of the nucleation process at P=2. The key configurations on the MEP are shown in figure 4b-d, in which the atoms are coloured by the shear strain measured with respect to the initial state. The nucleation starts with an initial 16 layers of hexagonal phase (represented by H16). The saddle configuration in figure 4b shows that the nucleation is triggered by the localized shear deformation that comes from the relative shift between two adjacent layers of atoms, similar to the mechanism observed in the unit cell. Beyond the saddle point, the nucleation continues to grow into one layer of square phase, leading to a structure with remaining 15 layers of hexagonal phase (represented by H15) as shown in figure 4c, which corresponds to a local minimum in energy landscape.

The nucleated square layer lowers the system total enthalpy since the square phase has a lower enthalpy than the hexagonal phase at low pressures; meanwhile, the interface formed between two phases (i.e. phase boundary) increases the total enthalpy. This energetic competition results in the nucleation MEP plotted in figure 4a. After the formation of the first layer of square phase, the H15 structure has a higher enthalpy than the initial H16 structure. Based on the classical nucleation theory, the nucleation needs to grow to further lower the enthalpy. As a result, beyond another saddle point (whose configuration is shown in electronic supplementary material, figure S1), the second layer of the square phase is formed adjacent to the first one and the entire nucleation process is completed until the total enthalpy drops below the initial state, yielding a thermodynamically stable nucleus with double layers of square phase represented by H14. The nucleation barrier, defined as the height in enthalpy of the first hump in MEP, increases with pressure, as shown in figure 4d. Moreover, since the enthalpy difference between the square and hexagonal phases decreases as pressure increases at the low pressure domain, more square

Downloaded from https://royalsocietypublishing.org/ on 07 December 2022

layers have to be nucleated inside the nucleus to make the total enthalpy below the initial value. Therefore, it is found that the size of nucleus with square phase grows as pressure increases, as shown in electronic supplementary material, figure S2 at P = 2.5. Given the importance of nucleus in phase transition for both theoretical analysis and applications, we use this model two-dimensional system to demonstrate the combination of Dimer and NEB methods as a valuable approach to identify the atomic structure of the nucleus, aiming to guild the future studies on even more complex materials.

Next, we study the phase propagation after the nucleation. Based on the layer-by-layer fashion observed in the nucleation process, it is expected that the growth of new phase follows a continuous layer-by-layer propagation. Our simulations indeed show such a method of propagation, but only up to a particular configuration that contains 12 remaining hexagonal layers. The MEP of the complete phase transition process is plotted in figure 5a, where H12 is used to denote the critical configuration. Beyond H12, the Dimer calculation suggests a different propagation path with lower barriers. Along this new path, the propagation is assisted by the formation of a line defect inside the remaining hexagonal phase, as shown in figure 5b. The line defect is an inclined layer of square phase that is formed first inside the remaining 12 hexagonal layers, so the corresponding structure is denoted as H12/D in figure 5. In the subsequent process, the growth of the square phase occurs simultaneously towards both the top and bottom phase boundaries with very low barriers, so that there are two new square layers formed in one transition step, in contrast to the layer-by-layer propagation in which only one new layer is formed in one transition step. This leads to larger enthalpy drops on the MEP of the defectassisted propagation path. In figure 5b, it is noted that an unstable diamond structure is formed at the junction where the line defect intersects the phase boundary. Figure 5c shows that this diamond structure is cleaved by the local shear deformation during the propagation, and a pentagon structure is formed to trigger the intralayer phase propagation along both the top and bottom phase boundaries. Figure 5a shows that the defect assisted propagation proceeds up to H4 when only four layers of hexagonal phase remain in the system. Beyond H4, the propagation jumps back to layer-by-layer mode until the end of phase transition at H0 in which all 16 layers of hexagonal phase transform to square phase. As a comparison, the continuous layer-by-layer propagation path is calculated using the NEB method and is plotted in figure 5a with the dashed line. Clearly, the defect-assisted propagation path is more kinetically favourable. It is likely, without using the Dimer method to sufficiently search all the possible saddles, that the low barrier defect-assisted propagation path may be easily missed.

To further look into the phase propagation mechanism described earlier, barriers of the defect formation inside the remaining hexagonal phase are compared against the barriers to form a new sequential layer of square phase. As shown in figure 6, when the remaining hexagonal layer number is beyond 12, the barrier of defect formation becomes lower than the other one, which explains the switch in propagation path at H12. In addition, our simulation shows that the line defect becomes unstable inside the remaining four layers of hexagonal phase and spontaneously disappears upon energy relaxation, which is why the propagation path jumps back to the layer by layer at H4. Another question one may ask is whether the observed phase transition mechanism will change in a larger super cell with more layers of the hexagonal phase. It is noted that the nucleation and layer-by-layer propagation mechanism, as well as the critical configurations (H12/D and H4), are not dependent on the initial number of hexagonal layers. The only difference in a larger super cell is that the initial layer-by-layer propagation requires more transition steps before reaching the H12 configuration. Other than that, we expect that the propagation path remains the same.

(c) Phase nucleation and propagation at high pressure: square to hexagonal

The $S \to H$ phase transition at high pressure is also studied with the combined Dimer and NEB method using the same approach as described in §3b. Similar to the $H \to S$ transition, the nucleation of $S \to H$ transition is promoted by the localized shear deformation, which is followed

royalsocietypublishing.org/journal/rspa *Proc. R. Soc. A* **478**: 20220388

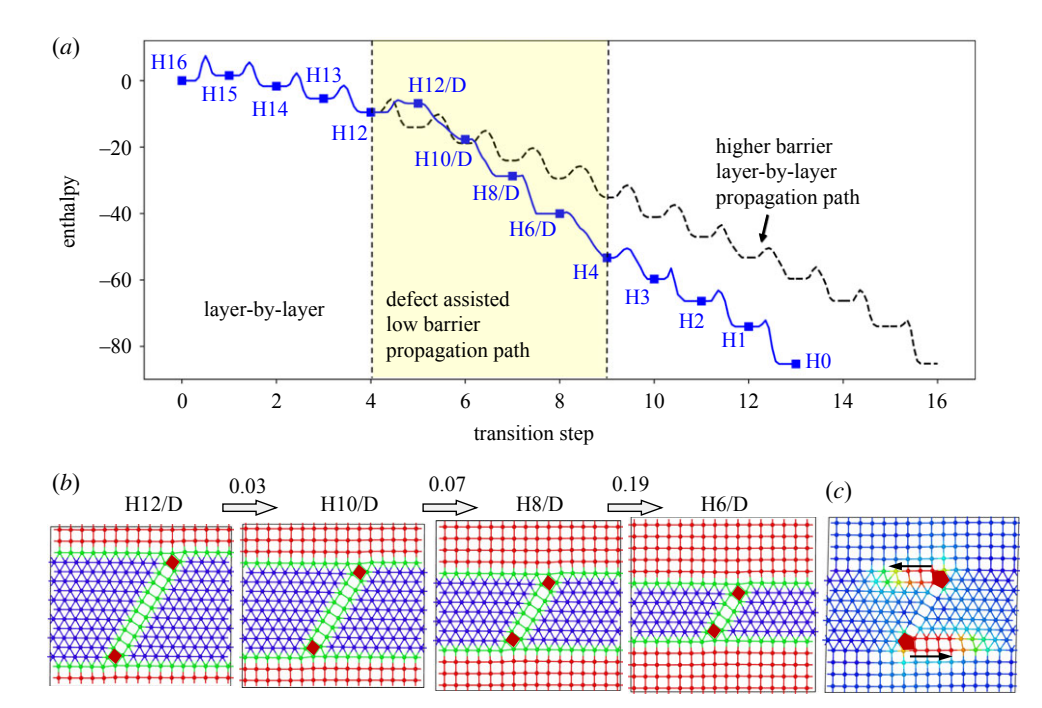


Figure 5. (a) The solid line shows the MEP of the complete transition process at P=2. H# represents the structure with # remaining hexagonal layers and H#/D represents H# with defect. The dashed line shows another MEP for the continuous layer-by-layer propagation. (b) Configurations of the defect inside hexagonal phase. Barriers between two configurations are labelled above the arrows. The phase propagation starts from the red coloured diamond structures formed at the junction of two phases. Atoms are coloured by the coordination number. (c) One intermediate configuration from H8/D to H6/D. The red coloured pentagons are cleaved from the diamonds in H8/D due to local shear deformation, triggering the intralayer propagation followed by the arrow direction. Atoms are coloured by shear strain ranged from 0 to 0.12. (Online version in colour.)

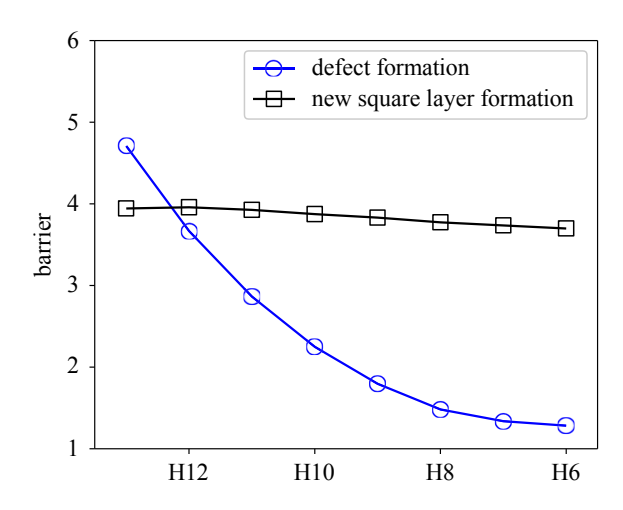


Figure 6. Comparison of barriers for defect formation and layer-by-layer propagation. (Online version in colour.)

by the layer-by-layer phase propagation. This process is illustrated by a saddle configuration shown as the inset of figure 7. The other inset in the figure plots the nucleation barriers of $S \to H$ transition, which drops as pressure increases. It is noted that one can use the barriers to estimate the phase transition rate based on the transition state theory. Under a harmonic approximation, the phase transition rate, k, can be estimated in terms of $k = v \exp[-E(P)/k_BT]$, where E is the

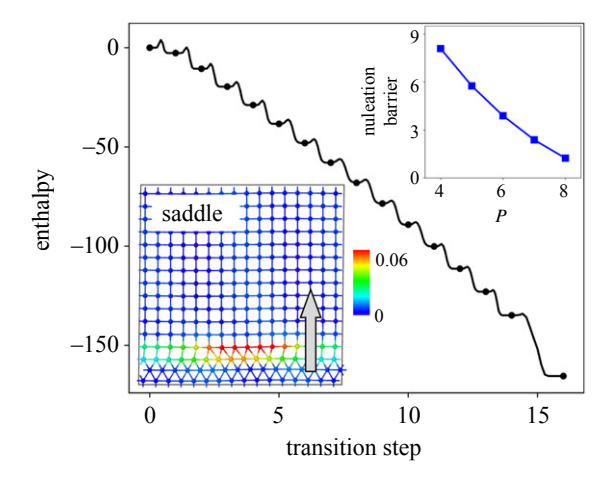


Figure 7. The MEP for $S \to H$ transition at P = 6. The insets show a saddle structure where atoms are coloured by shear strain, and the nucleation barriers as a function of pressure. (Online version in colour.)

barrier as a function of pressure P, k_B is the Boltzmann constant, T is the temperature and the prefactor ν is related to the atomic vibrational frequency and on the order of 10^{13} s⁻¹. In addition, the critical phase transition pressure can also be estimated with a given temperature and phase transition rate.

A complete phase transition MEP is plotted for P=6 in figure 7. It shows that the total enthalpy drops below the initial value right after the first transition step. Therefore, in this case, the nucleus is formed when one layer of square phase transforms to hexagonal phase. Since the enthalpy difference between the square and hexagonal phase increases with pressure, the size of the nucleus increases only when pressure decreases, which is different from the $H \rightarrow S$ transition. In addition, the MEP in figure 7 shows a continuous layer-by-layer propagation path throughout the entire transition process without the formation of any defects. There are no other lower barrier propagation paths identified from the Dimer calculation.

4. Summary

In this article, NEB and Dimer methods are applied to study the phase transition of a model twodimensional system that is described by a modified LJ potential. Using unit cells, two pressure domains are identified for hexagonal-to-square and square-to-hexagonal phase transitions. In addition, the concerted transition is found to be dependent on both atomic and cell degrees of freedom. By using a large super cell, it is found that the phase nucleation is triggered by the localized shear deformation that comes from the relative shift between two adjacent atomic layers. Two phase propagation mechanisms are identified: the conventional layer-by-layer phase propagation and a more interesting defect assisted low barrier propagation. The results of this study can be potentially applied to understand the phase transition in two-dimensional and quasi-two-dimensional solid-state and colloidal systems, when the interatomic or interparticle interactions in such systems can be described by a similar LJ potential used in this study. Although temperature is not involved in NEB and Dimer calculations, it plays a role in computing the rate of phase transition by using the Arrhenius equation with the inputs of the barriers calculated in the present work. The reported phase transition mechanism is not expected to be influenced by temperature, as long as the temperature is well below the melting point when the entropic contribution is not dominated. Finally, this article aims to present an exemplary study of phase transition in terms of the methodology, emphasizing the importance of combining the Dimer and NEB methods to efficiently and sufficiently probe the nucleation and propagation mechanism. An extension of the current study to include interactions between defects and phase transition is of great interest in the future, which can be done with a similar approach applied in this article.

royalsocietypublishing.org/journal/rspa Proc. R. Soc. A **478**: 20220388

Data accessibility. The data is available for download from Github https://github.com/Gao-Group/datapaper-phase-transition-2D-model-system. The supporting figures are provided in electronic supplementary material [39].

Authors' contributions. F.S.: data curation, investigation, methodology, software, writing—original draft and writing-review and editing; P.X.: investigation, methodology and writing-review and editing; L.X.: investigation and writing-review and editing; W.G.: conceptualization, data curation, formal analysis, funding acquisition, investigation, methodology, project administration, software, supervision, writingoriginal draft and writing—review and editing.

All authors gave final approval for publication and agreed to be held accountable for the work performed therein.

Conflict of interest declaration. We declare we have no competing interests.

Funding. W.G. and F.S. gratefully acknowledge financial support of this work by the National Science Foundation through Grant no. CMMI-1930783 and CMMI-2046218.

Acknowledgements. The authors acknowledge the Texas Advanced Computing Center (TACC) at the University of Texas at Austin for providing HPC resources that have contributed to the research results reported within this paper.

References

PhysRevB.88.144102)

- 1. Olijnyk H, Sikka S, Holzapfel W. 1984 Structural phase transitions in Si and Ge under pressures up to 50 GPa. Phys. Lett. A 103, 137–140. (doi:10.1016/0375-9601(84)90219-6)
- 2. Ghosh SK, Böker A. 2019 Self-assembly of nanoparticles in 2D and 3D: recent advances and future trends. Macromol. Chem. Phys. 220, 1900196. (doi:10.1002/macp.v220.17)
- 3. Egusa S, Redmond PL, Scherer NF. 2007 Thermally-driven nanoparticle array growth from atomic Au precursor solutions. J. Phys. Chem. C 111, 17 993–17 996. (doi:10.1021/jp076720a)
- 4. Brunner M, Bechinger C. 2002 Phase behavior of colloidal molecular crystals on triangular light lattices. Phys. Rev. Lett. 88, 248302. (doi:10.1103/PhysRevLett.88.248302)
- 5. Zittartz J. 1976 Phase transition of the two-dimensional classicalxy-model. Z. Phys. B Condens. Matter 23, 55–62. (doi:10.1007/BF01322261)
- 6. Damasceno PF, Gonçalves LGV, Rino JP, De Oliveira RDCM. 2009 Pressure-induced structural phase transitions in a two-dimensional system. Phys. Rev. B—Condens. Matter Mater. Phys. 79, 1–6. (doi:10.1103/PhysRevB.79.104109)
- 7. Lee KY, Ray JR. 1989 Mechanism of pressure-induced martensitic phase transformations: a molecular-dynamics study. Phys. Rev. B 39, 565-574. (doi:10.1103/PhysRevB.39.565)
- 8. Gränz B, Korshunov SE, Geshkenbein VB, Blatter G. 2016 Competing structures in two dimensions: square-to-hexagonal transition. Phys. Rev. B 94, 054110. (doi:10.1103/ PhysRevB.94.054110)
- 9. Khaliullin RZ, Eshet H, Kühne TD, Behler J, Parrinello M. 2011 Nucleation mechanism for the direct graphite-to-diamond phase transition. *Nat. Mater.* **10**, 693–697. (doi:10.1038/nmat3078)
- 10. Voter AF. 1998 Parallel replica method for dynamics of infrequent events. Phys. Rev. B 57, R13985–R13988. (doi:10.1103/PhysRevB.57.R13985)
- 11. Laio A, Parrinello M. 2002 Escaping free-energy minima. Proc. Natl Acad. Sci. USA 99, 12562-12566. (doi:10.1073/pnas.202427399)
- 12. Badin M, Martoňák R. 2021 Nucleating a different coordination in a crystal under pressure: a study of the b 1- b 2 transition in NaCl by metadynamics. Phys. Rev. Lett. 127, 105701. (doi:10.1103/PhysRevLett.127.105701)
- 13. Zhang L, Ren W, Samanta A, Du Q. 2016 Recent developments in computational modelling of nucleation in phase transformations. NPJ Comput. Mater. 2, 1–9. (doi:10.1038/ s41524-016-0001-z)
- 14. Ghasemi A, Gao W. 2020 Atomistic mechanism of stress modulated phase transition in monolayer MoTe2. Extr. Mech. Lett. 40, 100946. (doi:10.1016/j.eml.2020.100946)
- 15. Ghasemi A, Gao W. 2020 A method to predict energy barriers in stress modulated solid-solid phase transitions. *J. Mech. Phys. Solids* **137**, 1–13. (doi:10.1016/j.jmps.2019.103857)
- 16. Xiao P, Henkelman G. 2012 Communication: from graphite to diamond: reaction pathways of the phase transition. J. Chem. Phys. 137, 101101. (doi:10.1063/1.4752249)
- 17. Xiao P, Cheng J-G, Zhou J-S, Goodenough JB, Henkelman G. 2013 Mechanism of the CaIrO₃ post-perovskite phase transition under pressure. Phys. Rev. B 88, 144102. (doi:10.1103/

- 18. Jónsson H, Mills G, Jacobsen KW. 1998 Nudged elastic band method for finding minimum energy paths of transitions. In *Classical and Quantum Dynamics in Condensed Phase Simulations* (eds BJ Berne, G Ciccotti, DF Coker), pp. 385–404. Singapore: World Scientific. (doi:10.1142/9789812839664_0016)
- Henkelman G, Jónsson H. 2000 Improved tangent estimate in the nudged elastic band method for finding minimum energy paths and saddle points. J. Chem. Phys. 113, 9978–9985. (doi:10.1063/1.1323224)
- 20. Sheppard D, Xiao P, Chemelewski W, Johnson DD, Henkelman G. 2012 A generalized solid-state nudged elastic band method. *J. Chem. Phys.* **136**, 074103. (doi:10.1063/1.3684549)
- 21. Ghasemi A, Xiao P, Gao W. 2019 Nudged elastic band method for solid-solid transition under finite deformation. *J. Chem. Phys.* **151**, 054110. (doi:10.1063/1.5113716)
- 22. Ghasemi A, Gao W. 2021 A method to apply Piola-Kirchhoff stress in molecular statics simulation. *Comput. Mater. Sci.* **195**, 110496. (doi:10.1016/j.commatsci.2021.110496)
- 23. Henkelman G, Jónsson H. 1999 A dimer method for finding saddle points on high dimensional potential surfaces using only first derivatives. *J. Chem. Phys.* **111**, 7010–7022. (doi:10.1063/1.480097)
- 24. Xiao P, Sheppard D, Rogal J, Henkelman G. 2014 Solid-state dimer method for calculating solid-solid phase transitions. *J. Chem. Phys.* **140**, 174104. (doi:10.1063/1.4873437)
- 25. Mei D, Xu L, Henkelman G. 2008 Dimer saddle point searches to determine the reactivity of formate on Cu(111). *J. Catal.* 258, 44–51. (doi:10.1016/j.jcat.2008.05.024)
- 26. Henkelman G, Jónsson H. 2003 Multiple time scale simulations of metal crystal growth reveal the importance of multiatom surface processes. *Phys. Rev. Lett.* **90**, 4. (doi:10.1103/PhysRevLett.90.116101)
- Pedersen A, Pizzagalli L, Jónsson H. 2009 Finding mechanism of transitions in complex systems: formation and migration of dislocation kinks in a silicon crystal. *J. Phys. Condens. Matter* 21, 084210. (doi:10.1088/0953-8984/21/8/084210)
- 28. Weinan E, Ren W, Vanden-Eijnden E. 2002 String method for the study of rare events. *Phys. Rev. B* **66**, 052301. (doi:10.1103/PhysRevB.66.052301)
- 29. Weinan E, Ren W, Vanden-Eijnden E. 2007 Simplified and improved string method for computing the minimum energy paths in barrier-crossing events. *J. Chem. Phys.* **126**, 164103. (doi:10.1063/1.2720838)
- 30. Yin J, Zhang L, Zhang P. 2019 High-index optimization-based shrinking dimer method for finding high-index saddle points. *SIAM J. Sci. Comput.* **41**, A3576–A3595. (doi:10.1137/19M1253356)
- 31. Yin J, Wang Y, Chen JZ, Zhang P, Zhang L. 2020 Construction of a pathway map on a complicated energy landscape. *Phys. Rev. Lett.* **124**, 090601. (doi:10.1103/PhysRevLett. 124.090601)
- 32. Vanden-Eijnden E *et al.* 2010 Transition-path theory and path-finding algorithms for the study of rare events. *Annu. Rev. Phys. Chem.* **61**, 391–420. (doi:10.1146/physchem. 2010.61.issue-1)
- 33. Henkelman G, Jóhannesson G, Jónsson H. 2002 Methods for finding saddle points and minimum energy paths. In *Theoretical methods in condensed phase chemistry*, pp. 269–302. Berlin: Springer.
- 34. Heyden A, Bell AT, Keil FJ. 2005 Efficient methods for finding transition states in chemical reactions: comparison of improved dimer method and partitioned rational function optimization method. *J. Chem. Phys.* **123**, 224101. (doi:10.1063/1.2104507)
- 35. Larsen AH *et al.* 2017 The atomic simulation environment—a python library for working with atoms. *J. Phys.: Condens. Matter* **29**, 273002. (doi:10.1088/1361-648X/aa680e)
- 36. Plimpton S. 1995 Fast parallel algorithms for short-range molecular dynamics. *J. Comput. Phys.* **117**, 1–19. (doi:10.1006/jcph.1995.1039)
- 37. Xu L, Henkelman G. 2008 Adaptive kinetic Monte Carlo for first-principles accelerated dynamics. *J. Chem. Phys.* **129**, 114104. (doi:10.1063/1.2976010)
- 38. Stukowski A. 2010 Visualization and analysis of atomistic simulation data with OVITO—the Open Visualization Tool. *Modell. Simul. Mater. Sci. Eng.* **18**, 015012. (doi:10.1088/0965-0393/18/1/015012)
- 39. Shuang F, Xiao P, Xiong L, Gao W. 2022 Atomistic mechanisms of phase nucleation and propagation in a model two-dimensional system. Figshare. (doi:10.6084/m9.figshare. c.6316500)